

Validity of Image Theorems under Spherical Geometry

Shaolin Liao¹, Sasan Bakhtiari¹, and Henry Soekmadji²

¹Argonne National Laboratory, USA

²Hamilton Sundstrand, USA

Abstract— This paper deals with different image theorems, i.e., Love’s equivalence principle, the induction equivalence principle and the physical optics equivalence principle, in the spherical geometry. The deviation of image theorem approximation is quantified by comparing the modal expansion coefficients between the electromagnetic field obtained from the image approximation and the exact electromagnetic field for the spherical geometry. Two different methods, i.e., the vector potential method through the spherical addition theorem and the dyadic Green’s function method, are used to do the analysis. Applications of the spherical imaging theorems include metal mirror design and other electrically-large object scattering.

1. INTRODUCTION

Different image theorems have been widely used for electromagnetic modeling of mirrors and lens antenna [1]-[20]. In [20], Rong and Perkins applied the image theorems to mirror system design for high-power gyrotrons. The author also theoretically evaluate the validity of the image theorems in the cylindrical geometry [1]. In this article, following similar procedures in [1], a closed-form formula for the discrepancy parameter, which is defined as the ratio of the spherical modal coefficient for image theorem to that of the exact field, has been derived for the spherical geometry.

2. IMAGE THEOREMS IN THE SPHERICAL GEOMETRY

Fig. 1 shows the spherical geometry for image theorem analysis.

The Vector Potential Method

The spherical modal expansion In spherical coordinates, the electrical vector potential $\mathbf{F}(\mathbf{r})$ for $\mathbf{M}_s(\mathbf{r}')$ is given as [21], [22],

$$\mathbf{F}(\mathbf{r}) = \epsilon_0 \iint_{S'} dS' \mathbf{M}_s(\mathbf{r}') g(\mathbf{r} - \mathbf{r}') = \frac{-jk\epsilon_0}{4\pi} \iint_{S'} dS' \mathbf{M}_s(\mathbf{r}') h_0^{(2)}(k[r - r']) \quad (1)$$

where, $h_0^{(2)}$ is spherical Hankel function of the second kind of order 0. According to the spherical addition theorem [21], [22],

$$h_0^{(2)}(k[r - r']) = \sum_{n=0}^{\infty} (2n + 1) j_n(kr') h_n^{(2)}(kr) \quad (2)$$

$$\times \sum_{m=0}^n (2 - \delta_m^0) \frac{(n - m)!}{(n + m)!} P_n^m(\theta') P_n^m(\theta) \cos m(\phi - \phi')$$

where, j_n is the spherical Bessel function of the first kind of integral order n ; P_n^m is the associated Legendre polynomial and δ_m^0 is the Kronecker delta function ($\delta_m^0 = 1$ for $m=0$ and $\delta_m^0 = 0$ for $m \neq 0$). Substituting (2) into (1), the modal expansion of $\mathbf{F}(\mathbf{r})$ is obtained as,

$$\begin{aligned} \mathbf{F}(\mathbf{r}) &= \sum_{n=0}^{\infty} \sum_{m=0}^n \mathbf{f}_{\text{TE}}^{\text{Ms}}(n, m) h_n^{(2)}(kr) P_n^m(\theta) \begin{matrix} \cos m\phi \\ \sin m\phi \end{matrix} \\ \mathbf{f}_{\text{TE}}^{\text{Ms}} &= \chi \iint_{S'} dS' \mathbf{M}_s(\mathbf{r}') j_n(kr') P_n^m(\theta') \begin{matrix} \cos m\phi' \\ \sin m\phi' \end{matrix} \\ \chi &= (2 - \delta_m^0) \frac{-jk\epsilon_0}{4\pi} \frac{(2n + 1)(n - m)!}{(n + m)!} . \end{aligned} \quad (3)$$

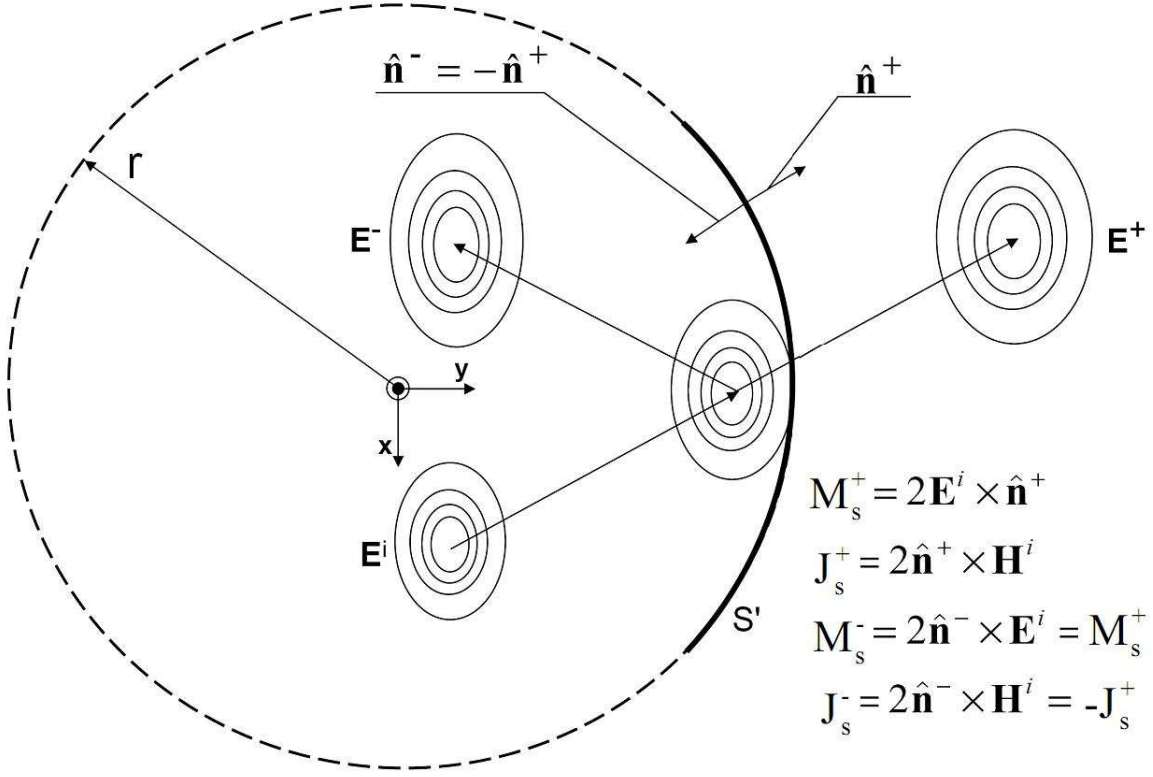


Figure 1: Image theorem in the spherical geometry: the incident field \mathbf{E}^i propagates onto spherical surface S' , then it may forward-propagate to \mathbf{E}^+ or it could be back-scattered to \mathbf{E}^- , depending on whether surface S' as a fictitious surface where the equivalence theorem applies on a PEC surface. $\hat{\mathbf{n}}^+$ and $\hat{\mathbf{n}}^-$ are the outward and inward surface normals on spherical surface S' respectively. \mathbf{M}_s and \mathbf{J}_s are equivalent surface currents for Love's equivalence theorem. \mathbf{M}_s^+ is the image approximation of Love's theorem and \mathbf{M}_s^- is the image approximation for the induction theorem.

The near field to far field transform of (3) in the spherical coordinate is given as [23],

$$\mathbf{F}(\mathbf{r}) \Big|_{r \rightarrow \infty} = \frac{j e^{-jkr}}{kr} \sum_{n=0}^{\infty} \sum_{m=0}^n j^n \mathbf{f}_{\text{TE}}^{\mathbf{M}_s}(n, m) P_n^m(\theta) \begin{array}{l} \cos m\phi \\ \sin m\phi \end{array} \quad (4)$$

The duality relation can be used to obtain the magnetic vector potential $\mathbf{A}(\mathbf{r})$ for the \mathbf{J}_s approximation as follows,

$$\begin{aligned} \mathbf{A}(\mathbf{r}) &= \sum_{n=0}^{\infty} \sum_{m=0}^n \mathbf{g}_{\text{TE}}^{\mathbf{M}_s}(n, m) h_n^{(2)}(kr) P_n^m(\theta) \begin{array}{l} \cos m\phi \\ \sin m\phi \end{array} \\ \mathbf{g}_{n, \text{TE}}^{m, \mathbf{M}_s} &= \chi' \iint_{S'} dS' \mathbf{J}_s(\mathbf{r}') j_n(kr') P_n^m(\theta') \begin{array}{l} \cos m\phi' \\ \sin m\phi' \end{array} \\ \chi' &= (2 - \delta_m^0) \frac{-jk\mu_0}{4\pi} \frac{(2n+1)(n-m)!}{(n+m)!} . \end{aligned} \quad (5)$$

The back-scattered and forward-propagating waves Similar to the cylindrical geometry, we can separate (3) into back-scattered and forward-propagating waves as,

$$j_n(kr') = \frac{1}{2} \left\{ h_n^{(1)}(kr') + h_n^{(2)}(kr') \right\} \quad (6)$$

$$\mathbf{f}_{n, \text{TE}}^{m, \mathbf{M}_s \pm} = \frac{\chi}{2} \iint_{S'} dS' \mathbf{M}_s(\mathbf{r}') h_n^{(1), (2)}(kr') P_n^m(\theta') \begin{array}{l} \cos m\phi' \\ \sin m\phi' \end{array}$$

Since the spherical harmonics is a complete basis set, we can always express the initial incident electric field $\mathbf{E}(\mathbf{r}')$ on the initial spherical surface S' with radius of r_0 (in Figure 1) as follows,

$$\begin{aligned}\mathbf{E}(\mathbf{r}_0) &= \sum_{n=0}^{\infty} \sum_{m=0}^n a_{n,o}^{m,e} \mathbf{M}_{n,o}^{m,e+}(\mathbf{r}_0) + b_{n,o}^{m,e} \mathbf{N}_{n,o}^{m,e+}(\mathbf{r}_0) \\ \psi_{n,o}^{m,e+}(\mathbf{r}_0) &= h_m^{(2)}(kr_0) P_n^m(\cos \theta') \frac{\cos(m\phi')}{\sin(m\phi')} \\ \mathbf{L}_{n,o}^{m,e+}(\mathbf{r}_0) &= \nabla \psi_{n,o}^{m,e+}(\mathbf{r}_0) \\ \mathbf{M}_{n,o}^{m,e+}(\mathbf{r}_0) &= \nabla \times \{ \mathbf{a}_r r \psi_{n,o}^{m,e+}(\mathbf{r}_0) \} \\ \mathbf{N}_{n,o}^{m,e+}(\mathbf{r}_0) &= \frac{1}{k} \nabla \times \mathbf{M}_{n,o}^{m,e+}(\mathbf{r}_0) .\end{aligned}\quad (7)$$

From (3) and noting that $\mathbf{M}_s^+(\mathbf{r}_0) = 2\mathbf{E}(\mathbf{r}_0) \times \mathbf{a}_r$, on spherical surface S' in Figure 1,

$$\begin{aligned}\tilde{\mathbf{E}}(\mathbf{r}_0) &= -\frac{1}{\epsilon_0} \sum_{n=0}^{\infty} \sum_{m=0}^n \{ \mathbf{L}_{n,o}^{m,e+}(\mathbf{r}) \times \mathbf{f}_{n,\text{TE}}^{m,\mathbf{M}_s} \} \\ \mathbf{L}_{n,o}^{m,e+}(\mathbf{r}_0) &= \nabla \psi_{n,o}^{m,e+}(\mathbf{r}_0)\end{aligned}\quad (8)$$

The approximate field $\tilde{\mathbf{E}}(\mathbf{r}_0)$ on the initial spherical surface S' is obtained from (3) through image theorem approximation,

$$\tilde{\mathbf{E}}(\mathbf{r}_0) = \sum_{n=0}^{\infty} \sum_{m=0}^n \tilde{a}_{n,o}^{m,e} \mathbf{M}_{n,o}^{m,e}(\mathbf{r}_0) + \tilde{b}_{n,o}^{m,e} \mathbf{N}_{n,o}^{m,e+}(\mathbf{r}_0) \quad (9)$$

Now the deviation of the spherical coefficients $\tilde{a}_{n,o}^{m,e}, \tilde{b}_{n,o}^{m,e}$ in Eq. (9) from their exact values $a_{n,o}^{m,e}, b_{n,o}^{m,e}$ in Eq. (7) is defined as the discrepancy parameters ζ ,

$$\begin{aligned}\zeta_{\text{TE}}^{\mathbf{M}_s} &= \frac{\tilde{a}_{n,o}^{m,e}}{a_{n,o}^{m,e}} = -j2kr_0 h_n^{(2)}(kr_0) \frac{\partial [kr j_n(kr)]}{\partial kr} \Big|_{r=r_0} \\ \zeta_{\text{TM}}^{\mathbf{M}_s} &= \frac{\tilde{b}_{n,o}^{m,e}}{b_{n,o}^{m,e}} = j2kr_0 j_n(kr_0) \frac{\partial [kr h_n^{(2)}(kr)]}{\partial kr} \Big|_{r=r_0}\end{aligned}$$

and,

$$\begin{aligned}\zeta_{\text{TE}}^{\mathbf{M}_s, \pm} &= -j2kr_0 h_n^{(2)}(kr_0) \frac{\partial [kr h_n^{(1),(2)}(kr)]}{\partial kr} \Big|_{r=r_0} \\ \zeta_{\text{TM}}^{\mathbf{M}_s, \pm} &= j2kr_0 h_n^{(1),(2)}(kr_0) \frac{\partial [kr h_n^{(2)}(kr)]}{\partial kr} \Big|_{r=r_0} .\end{aligned}\quad (10)$$

Similar expressions exist for \mathbf{J}_s image approximation,

$$\zeta_{\text{TE}}^{\mathbf{J}_s} = \zeta_{\text{TM}}^{\mathbf{M}_s}, \quad \zeta_{\text{TM}}^{\mathbf{J}_s} = \zeta_{\text{TE}}^{\mathbf{M}_s} \quad (11)$$

$$\zeta_{\text{TE}}^{\mathbf{M}_s, \pm} = \zeta_{\text{TM}}^{\mathbf{J}_s, \pm} = [\zeta_{\text{TE}}^{\mathbf{J}_s, \pm}]^* = [\zeta_{\text{TM}}^{\mathbf{M}_s, \pm}]^* .$$

The Dyadic Green's Function Method The magnetic dyadic Green's function in the spherical coordinate is,

$$\bar{\mathbf{G}}_m(\mathbf{r}, \mathbf{r}') = -\frac{\mathbf{a}_r \mathbf{a}_r}{k^2} \delta(\mathbf{r} - \mathbf{r}') - \sum_{n=-\infty}^{\infty} \frac{j\pi}{2kn(n+1)}$$

Table 1: Summary of $\zeta_{\text{TE, TM}}^{\pm, -}(\mathbf{m}_s, \mathbf{j}_s)$ for the spherical geometry

TE/TM modes and $\mathbf{M}_s/\mathbf{J}_s$	The relations	$\zeta_{\text{TE, TM}}^{\pm, -}(\mathbf{M}_s, \mathbf{J}_s)$	$r_0 \rightarrow \infty$
TE & \mathbf{M}_s / TM & \mathbf{J}_s			
Sphere: back-scattered wave	$\zeta_{\text{TE}}^-(\mathbf{M}_s) = \zeta_{\text{TM}}^-(\mathbf{J}_s)$	$-jkr_0 h_n^{(2)}(kr_0) \frac{\partial [kr h_n^{(2)}(kr)]}{\partial kr} \Big _{r=r_0}$	$(-1)^n e^{-j2kr_0}$
Sphere: forward-propagating wave	$\zeta_{\text{TE}}^+(\mathbf{M}_s) = \zeta_{\text{TM}}^+(\mathbf{J}_s)$	$-jkr_0 h_n^{(2)}(kr_0) \frac{\partial [kr h_n^{(1)}(kr)]}{\partial kr} \Big _{r=r_0}$	1
TM & \mathbf{M}_s / TE & \mathbf{J}_s			
Sphere: back-scattered wave	$\zeta_{\text{TM}}^-(\mathbf{M}_s) = \zeta_{\text{TE}}^-(\mathbf{J}_s)$	$jkr_0 h_n^{(2)}(kr_0) \frac{\partial [kr h_n^{(2)}(kr)]}{\partial kr} \Big _{r=r_0}$	$-(-1)^n e^{-j2kr_0}$
Sphere: forward-propagating wave	$\zeta_{\text{TM}}^+(\mathbf{M}_s) = \zeta_{\text{TE}}^+(\mathbf{J}_s)$	$[\zeta_{\text{TE}}^+(\mathbf{M}_s)]^* / [\zeta_{\text{TM}}^+(\mathbf{J}_s)]^*$	1

$$\times \sum_{m=0}^n \frac{1}{Q_{nm}} \{ \mathbf{M}_{n,o}^{m,e}(\mathbf{r}') \mathbf{M}_{n,o}^{m,e+}(\mathbf{r}) + \mathbf{N}_{n,o}^{m,e}(\mathbf{r}') \mathbf{N}_{n,o}^{m,e+}(\mathbf{r}) \}$$

and,
$$Q_{nm} = \frac{2\pi^2(n+m)!}{(2-\delta_m^0)(2n+1)(n-m)!} \quad (12)$$

where $\mathbf{M}_{n,o}^{m,e}$ ($\mathbf{N}_{n,o}^{m,e}$) is obtained by replacing $h_n^{(2)}$ with j_n in $\mathbf{M}_{n,o}^{m,e+}$ ($\mathbf{N}_{n,o}^{m,e+}$). The approximate field $\tilde{\mathbf{E}}(\mathbf{r})$ for $\mathbf{M}_s^+(\mathbf{r}')$ is given as,

$$\tilde{\mathbf{E}}(\mathbf{r}) = -\nabla \times \iint_{S'} dS' \mathbf{M}_s^+(\mathbf{r}') \cdot \bar{\mathbf{G}}_m(\mathbf{r}, \mathbf{r}') \quad (13)$$

Substituting (12) into (13) and using the orthogonal properties of spherical modal functions, the approximate field $\tilde{\mathbf{E}}(r_0)$ on initial spherical surface S' is obtained as,

$$\begin{aligned} \tilde{\mathbf{E}}(r_0) = & \sum_{n=-\infty}^{\infty} \sum_{m=0}^n \frac{j\pi}{n(n+1)Q_{nm}} \frac{c_{n,o}^{m,e} \mathbf{M}_{n,o}^{m,e+}(\mathbf{r})}{d_{n,o}^{m,e} \mathbf{N}_{n,o}^{m,e+}(\mathbf{r})} \\ & \times \iint_{S'} dS' \frac{[\mathbf{N}_{n,o}^{m,e}(\mathbf{r}')]^* \times \mathbf{M}_{n,o}^{m,e+}(\mathbf{r}')}{[\mathbf{M}_{n,o}^{m,e}(\mathbf{r}')]^* \times \mathbf{N}_{n,o}^{m,e+}(\mathbf{r}')} \cdot \mathbf{a}_{r'} . \end{aligned} \quad (14)$$

The evaluation of (14) also leads to (9) and (10).

The Analytical Formula for Image Theorems in the Spherical Geometry Similar to the cylindrical geometry, $\zeta_{\text{TE, TM}}^{\mathbf{M}_s, \mathbf{J}_s \pm}$ in (10) and (11) can be considered as theoretical formulas for evaluation of the image theorems for narrow-band fields in the spherical geometry. The large argument asymptotic behaviors of $\zeta_{\text{TE, TM}}^{\mathbf{M}_s, \mathbf{J}_s \pm}$ for $r_0 \rightarrow \infty$ can be obtained by noting that,

$$\begin{aligned} h_n^{(2)}(kr_0) = [h_n^{(1)}(kr_0)]^* & \sim \frac{1}{kr_0} j^{(n+1)} e^{-jkr_0}, \quad kr_0 \rightarrow \infty \\ \zeta_{\text{TE, TM}}^{\mathbf{M}_s, \mathbf{J}_s \pm} \Big|_{r_0 \rightarrow \infty} & = 1 . \end{aligned} \quad (15)$$

3. RESULTS AND DISCUSSION

TABLE 1 summarizes the properties of $\zeta_{\text{TE, TM}}^{\mathbf{M}_s, \mathbf{J}_s \pm}$, for the back-scattered and forward-propagating waves respectively. For $r_0 \rightarrow \infty$, $\zeta_{\text{TE, TM}}^{\mathbf{M}_s, \mathbf{J}_s} = \zeta_{\text{TE, TM}}^{\mathbf{M}_s, \mathbf{J}_s +} + \zeta_{\text{TE, TM}}^{\mathbf{M}_s, \mathbf{J}_s -}$ shows fast oscillations, which can be

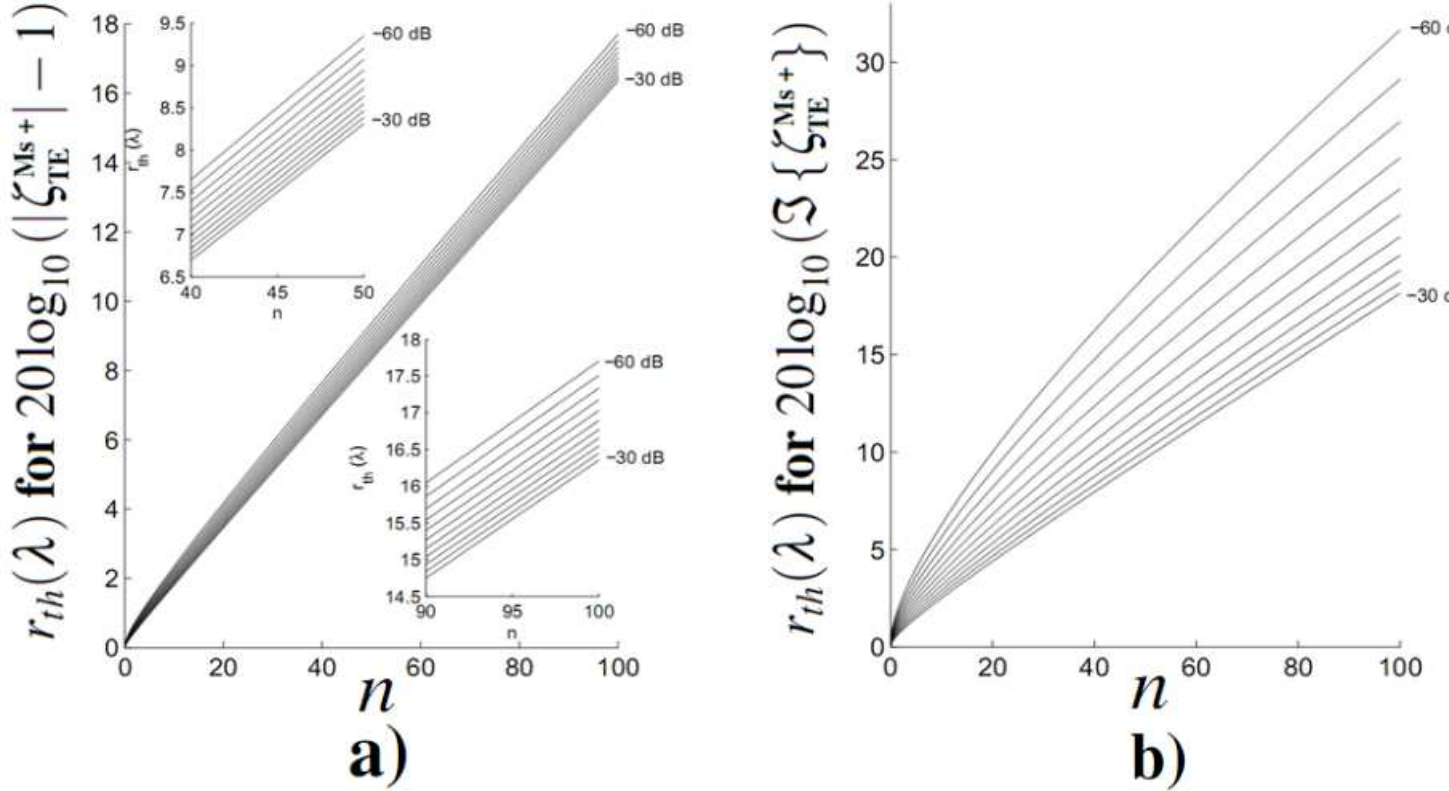


Figure 2: The spherical geometry - threshold radii r_{th} Vs. $n=0$ to 100 , for different accuracies, from -60 dB to -30 dB (in 10 dB increment, from bottom to top): a) the magnitudes $20 \log_{10}(|\zeta_{TE}^{Ms+}| - 1)$, and b) the imaginary parts $20 \log_{10}[\Im\{\zeta_{TE}^{Ms+}\}]$. The inset plots in a) are used to make the display clearer. Similar to the cylindrical geometry, imaginary parts ζ_{TE}^{Ms+} require larger threshold radii r_{th} for the same accuracy.

seen from TABLE 1. Mathematically, the oscillations only appear as modal expansion coefficients and disappear after the implementation of the double sums in (9). Physically, the oscillations are due to back-scattered fields, which approach 0 for $r_0 \rightarrow \infty$. For example, consider ζ_{TE}^{Ms-} in (10),

$$\tilde{\mathbf{E}}^-(r_0, \phi) = \sum_{n=0}^{\infty} \sum_{m=0}^n \{ \zeta_{TE}^{Ms-} c_{n,o}^{m,e} \mathbf{M}_{n,o}^{m,e+}(\mathbf{r}_0) + \zeta_{TE}^{Ms-} b_{n,o}^{m,e} \mathbf{N}_{n,o}^{m,e+}(\mathbf{r}_0) \} \quad (16)$$

Changing the variable $\phi' = \phi - \pi$ and letting $r_0 \rightarrow \infty$, from TABLE 1, (16) reduces to,

$$\tilde{\mathbf{E}}^-(r_0, \phi') \Big|_{r_0 \rightarrow \infty} = \sum_{n=0}^{\infty} \sum_{m=0}^n e^{-j2kr_0} \{ c_{n,o}^{m,e} \mathbf{M}_{n,o}^{m,e+}(\mathbf{r}_0) - b_{n,o}^{m,e} \mathbf{N}_{n,o}^{m,e+}(\mathbf{r}_0) \}. \quad (17)$$

Now, the back-scattered field $\tilde{\mathbf{E}}^-(r_0, \phi') \Big|_{r_0 \rightarrow \infty} \rightarrow 0$ due to the fast variation phase term e^{-j2kr_0} , which means that the oscillation in ζ_{TE}^{Ms-} doesn't appear in the actual field evaluation for $r_0 \rightarrow \infty$.

Based on the above discussion, $\zeta_{TE, TM}^{Ms, Js \pm}$ is the theoretical formula of interest to evaluate the validity of image theorems.

It is also helpful to plot the corresponding threshold radius r_{th} with respect to n , for both $20 \log_{10}(|\zeta_{TE}^{Ms+}| - 1)$ and $20 \log_{10}\{\Im[\zeta_{TE}^{Ms+}]\}$, with different accuracies ranging from -60 dB to -30 dB (in 3 dB increment), as in Fig. 2. It can be seen from Fig. 2 that, in order to achieve an accuracy of -30 dB for $|\zeta_{TE}^{Ms+}|$ (with respect to 1), $r_{th} \sim 8\lambda$ and $r_{th} \sim 16\lambda$ for $n = 50$ and $n = 100$ respectively. However, for the imaginary part $\Im[\zeta_{TE}^{Ms+}]$, $r_{th} \sim 9.5\lambda$ and $r_{th} \sim 18\lambda$ are required for $n = 50$ and $n = 100$ respectively, which again implies that the imaginary part ζ_{TE}^{Ms+} dominates the accuracy of image theorems.

4. CONCLUSION

For spherical geometry, the theoretical formulas for evaluation of the image theorems (both \mathbf{M}_s and \mathbf{J}_s approximations) have been derived through two equivalent methods - the vector potential method and the dyadic Green's function method, for both TE and TM modes. The ratio of the spherical modal coefficient of the image theorem to that of the exact field is used as the criterion to determine the validity of the image theorem.

REFERENCES

1. Shaolin Liao and R. J. Vernon, "On the Image Approximation for Electromagnetic Wave Propagation and PEC Scattering in Cylindrical Harmonics", *Progress In Electromagnetics Research*, PIER 66, 65-88, 2006.
2. Shaolin Liao, "Beam-shaping PEC Mirror Phase Corrector Design," *PIERS Online*, 3(4):392-396, 2007.
3. S.-L. Liao and R. J. Vernon, "A new fast algorithm for field propagation between arbitrary smooth surfaces", *the joint 30th Infrared and Millimeter Waves and 13th International Conference on Terahertz Electronics*, Williamsburg, Virginia, USA, 2005, ISBN: 0-7803-9348-1, INSPEC number: 8788764, DOI: 10.1109/ICIMW.2005.1572687, Vol. 2, pp. 606-607.
4. S.-L. Liao and R. J. Vernon, "The near-field and far-field properties of the cylindrical modal expansions with application in the image theorem," *the 31st Int. Conf. on Infrared and Millimeter Waves*, Shanghai, China, IEEE MTT, Catalog Number: 06EX1385C, ISBN: 1-4244-0400-2, Sep. 18-22, 2006.
5. S.-L. Liao and R. J. Vernon, "The cylindrical Taylor-interpolation FFT algorithm," *the 31st Int. Conf. on Infrared and Millimeter Waves*, Shanghai, China, IEEE MTT, Catalog Number: 06EX1385C, ISBN: 1-4244-0400-2, Sep. 18-22, 2006.
6. S.-L. Liao and R. J. Vernon, "Sub-THz beam-shaping mirror designs for quasi-optical mode converter in high-power gyrotrons", *J. Electromagn. Waves and Appl.*, scheduled for volume 21, number 4, page 425-439, 2007.
7. Shaolin Liao and R.J. Vernon, "A new fast algorithm for calculating near-field propagation between arbitrary smooth surfaces," In *2005 Joint 30th International Conference on Infrared and Millimeter Waves and 13th International Conference on Terahertz Electronics*, volume 2, pages 606-607 vol. 2, September 2005. ISSN: 2162-2035.
8. Shaolin Liao, Henry Soekmadji, and Ronald J. Vernon, "On Fast Computation of Electromagnetic Wave Propagation through FFT," In *2006 7th International Symposium on Antennas Propagation EM Theory*, pages 1-4, October 2006.
9. Shaolin Liao, "Fast Computation of Electromagnetic Wave Propagation and Scattering for Quasi-cylindrical Geometry," *PIERS Online*, 3(1):96-100, 2007.
10. Shaolin Liao, "On the validity of physical optics for narrow-band beam scattering and diffraction from the open cylindrical surface," *Progress in Electromagnetics Research Symposium (PIERS)*, vol. 3, no. 2, pp. 158162 Mar., 2007. arXiv:physics/3252668. DOI: 10.2529/PIERS060906142312
11. Shaolin Liao, Ronald J. Vernon, and Jeffrey Neilson, "A high-efficiency four-frequency mode converter design with small output angle variation for a step-tunable gyrotron," In *2008 33rd International Conference on Infrared, Millimeter and Terahertz Waves*, pages 1-2, September 2008. ISSN: 2162-2035.
12. S. Liao, R. J. Vernon, and J. Neilson, "A four-frequency mode converter with small output angle variation for a step-tunable gyrotron," In *Electron Cyclotron Emission and Electron Cyclotron Resonance Heating (EC-15)*, pages 477-482. WORLD SCIENTIFIC, April 2009.
13. Ronald J. Vernon, "High-Power Microwave Transmission and Mode Conversion Program," Technical Report DOEUW52122, Univ. of Wisconsin, Madison, WI (United States), August 2015.
14. Shaolin Liao, *Multi-frequency beam-shaping mirror system design for high-power gyrotrons: theory, algorithms and methods*, Ph.D. Thesis, University of Wisconsin at Madison, USA, 2008. AAI3314260 ISBN-13: 9780549633167.
15. Shaolin Liao and Ronald J. Vernon, "A Fast Algorithm for Wave Propagation from a Plane or a Cylindrical Surface," *International Journal of Infrared and Millimeter Waves*, 28(6):479-490, June 2007.

-
16. Shaolin Liao, "Miter Bend Mirror Design for Corrugated Waveguides," *Progress In Electromagnetics Research*, 10:157-162, 2009.
 17. Shaolin Liao and Ronald J. Vernon, "A Fast Algorithm for Computation of Electromagnetic Wave Propagation in Half-Space," *IEEE Transactions on Antennas and Propagation*, 57(7):2068-2075, July 2009.
 18. Shaolin Liao, N. Gopalsami, A. Venugopal, A. Heifetz, and A. C. Raptis, "An efficient iterative algorithm for computation of scattering from dielectric objects," *Optics Express*, 19(4):3304-3315, February 2011. Publisher: Optical Society of America.
 19. Shaolin Liao, "Spectral-domain MOM for Planar Meta-materials of Arbitrary Aperture Waveguide Array," In *2019 IEEE MTT-S International Conference on Numerical Electromagnetic and Multiphysics Modeling and Optimization (NEMO)*, pages 1-4, May 2019.
 20. Michael P. Perkins and Ronald J. Vernon, Iterative design of a cylinder-based beam-shaping mirror pair for use in a gyrotron internal quasi-optical mode converter, the 29th Int. Conf. on Infrared and Millimeter Waves, Karlsruhe, Germany, Sep. 27-Oct. 1, 2004.
 21. Roger F. Harrington, *Time-Harmonic Electromagnetic Fields*, McGraw-Hill, Inc., 1961.
 22. J. A. Stratton, *Electromagnetic Theory*, McGraw-Hill, Inc., 1941.
 23. A. D. Yaghjian, An overview of near-field antenna measurements, *IEEE Trans. on Antennas and Propagation*, 34(1) (1986) 30-45.